Results of the Department of Space Physics, Institute of Atmospheric Physics, Czech Academy of Sciences, published in 2022

1. Statistical analysis of wave propagation properties of equatorial noise observed at low altitudes

Equatorial noise is an electromagnetic emission with line spectral structure, predominantly located in the vicinity of the geomagnetic equatorial plane at radial distances ranging from 2 to 8 Earth's radii. Here we focus on the rare events of equatorial noise occurring at ionospheric altitudes during periods of strongly increased geomagnetic activity. We use multicomponent electromagnetic measurements from the entire 2004–2010 DEMETER spacecraft mission and present a statistical analysis of wave propagation properties. We show that, close to the Earth, these emissions experience a larger spread in latitudes than they would at large radial distances and that their wave normals can significantly deviate from the direction perpendicular to local magnetic field lines. These results are compared to ray tracing simulations, in which whistler mode rays with initially nearly perpendicular wave vectors propagate down to the low altitudes with wave properties corresponding to the observations. We perform nonlinear fitting of the simulated latitudinal distribution of incident rays to the observed occurrence and estimate the distribution of wave normal angles in the source. The assumed Gaussian distribution provides the best fit with a standard deviation of 2° from the perpendicular direction. Ray tracing analysis further shows that small initial deviations from the meridional plane can rapidly increase during the propagation and result in deflection of the emissions before they can reach the altitudes of DEMETER.

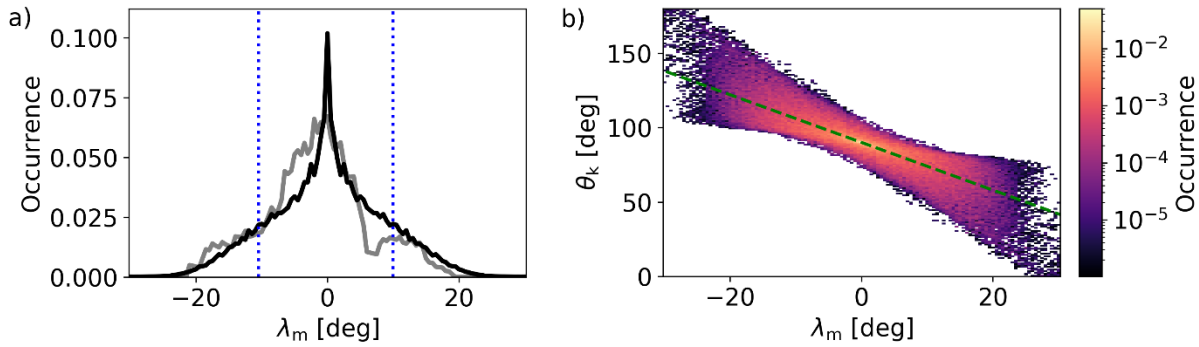

a) Distribution of equatorial noise in latitudes as observed by DEMETER (grey line) compared to the distribution of simulated incident rays (black line). Blue dotted lines show the quartiles of the simulated distribution. b) Distribution of incident rays in latitude and wave normal angles. Green dashed line represents a weighted linear fit.

Reference:

Hanzelka, M., Němec, F., **Santolík, O.**, & Parrot, M. (2022). Statistical analysis of wave propagation properties of equatorial noise observed at low altitudes. *Journal of Geophysical Research: Space Physics*, 127. doi:10.1029/2022JA030416.

2. Effects of Field-Aligned Cold Plasma Density Filaments on the Fine Structure of Chorus

The whistler-mode chorus emission, a major driver of radiation belt electron energization and precipitation, exhibits significant amplitude modulations on millisecond timescales. These subpacket modulations are accompanied by fast changes in the wave normal angle. Understanding the evolution of wave propagation properties inside chorus elements is essential for modeling nonlinear chorus-electron interactions, but the origin of these rapid changes is unclear. We propose that the variations come from propagation inside thin, field-aligned cold plasma enhancements (density ducts), which produce differing modulations in parallel and perpendicular wave magnetic field components. We show that a full-wave simulation on a filamented density background predicts wave vector and amplitude evolution similar to Van Allen Probes spacecraft observations. We further demonstrate that the commonly assumed wide density ducts, in which wave propagation can be studied with ray tracing methods, cannot explain the observed behavior. This indirectly proves the existence of wavelength-scale field-aligned density fluctuations.

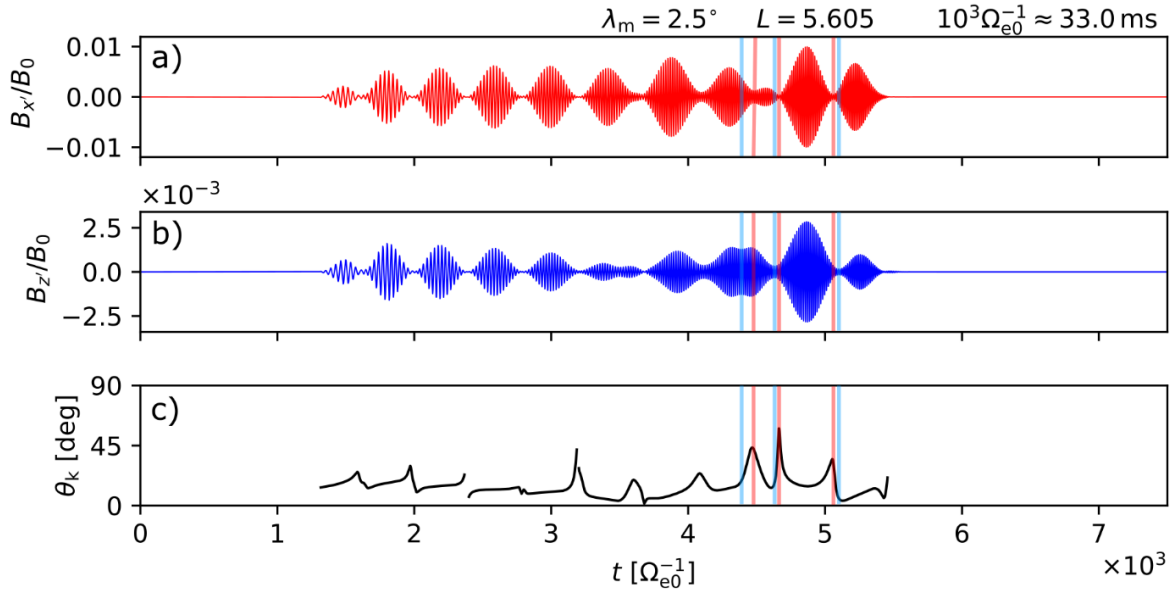

Results of full-wave simulation of a modulated rising-tone chorus element propagating from the equator in thin field-aligned density enhancements. a, b) Waveforms of parallel and perpendicular magnetic field recorded by a simulation probe at latitude of 2.5°. Blue and red vertical lines show the mismatch in amplitude minima of the last three subpackets. c) Wave normal angle computed from waveforms in previous panels. Largest deviations from parallel propagation appear where the magnetic field components experience the biggest mismatch in amplitude modulation.

Reference:

Hanzelka, M., & **Santolík, O.** (2022). Effects of Field-Aligned Cold Plasma Density Filaments on the Fine Structure of Chorus. *Geophysical Research Letters*, 49. doi:10.1029/2022GL101654.

Related references:

Hartley, D. P., Chen, L., Christopher, I. W., Kletzing, C. A., **Santolík, O.**, Li, W., & Shi, R. (2022). The angular distribution of lower band chorus waves near plasmaspheric plumes. *Geophysical Research Letters*, 49. doi:10.1029/2022GL098710.

Hartley, D. P., Christopher, I. W., Kletzing, C. A., Kurth, W. S., **Santolík, O.**, **Kolmašová, I.**, et al. (2022). Quantifying the sheath impedance of the electric double probe instrument on the Van Allen Probes. *Journal of Geophysical Research: Space Physics*, 127. doi:10.1029/2022JA030369.

Dahmen, N., Sicard, A., Brunet, A., **Santolik, O.**, Pierrard, V., Botek, E., et al. (2022). FARWEST: Efficient computation of wave-particle interactions for a dynamic description of the electron radiation belt diffusion. *Journal of Geophysical Research: Space Physics*, 127. doi:10.1029/2022JA030518

Rae, J., Forsyth, C. Dunlop, M., Palmroth, M. Lester, M. Friedel, R., …., **Santolík, O.** et al. (2022), What are the fundamental modes of energy transfer and partitioning in the coupled Magnetosphere-Ionosphere system?, *Experimental Astronomy*. doi:10.1007/s10686-022-09861-w.

Miyoshi, Y., Shinohara, I., Ukhorskiy, S., Claudepierre, S.G., Mitani, T., Takashima, T., Hori, T., **Santolík, O., Kolmašová, I.,** et al. (2022), Collaborative Research Activities of the Arase and Van Allen Probes, *Space Science Reviews*, 218:38. doi:10.1007/s11214-022-00885-4.

3. Lightning activity in northern Europe during a stormy winter: disruptions of weather patterns originating in global climate phenomena

In this study, we use the World Wide Lightning Location Network data and investigate properties of more than ninety thousand lightning strokes which hit Northern Europe during an unusually stormy winter 2014/2015. Thunderstorm days with at least two strokes hitting an area of 0.5° x 0.5° occurred 5-13 times per month in the stormiest regions. Such frequency of thunderstorm days is about five times higher than a mean annual number calculated for the same region over winter months in 2008-2017. The number of individual winter lightning strokes was about four times larger than the long-term median calculated over the last decade. In colder months of December, January and February, the mean energy of detected strokes was by two order of magnitude larger than the global mean stroke energy of 1 kJ. We show for the first time that winter superbolts with radiated electromagnetic energies above one mega joule appeared at night and in the morning hours, while the diurnal distribution of all detected lightning was nearly uniform. We also show that the superbolts were often single stroke flashes and that their subsequent strokes never reached MJ energies. The lightning strokes were concentrated above the ocean close to the western coastal areas. All these lightning characteristics suppose an anomalously efficient winter thundercloud charging in the eastern North Atlantic, especially at the sea-land boundary. We found that the resulting unusual production of lightning could not be explained solely by an anomalously warm sea surface caused by a positive phase of the North Atlantic Oscillation and by a starting super El Nino event. Increased updraft strengths, which are believed to accompany the cold to warm transition phase of El Nino, might have acted as another charging driver. We speculate that a combination of both these large-scale climatic events might have been needed to produce observed enormous amount of winter lightning in winter 2014/2015.

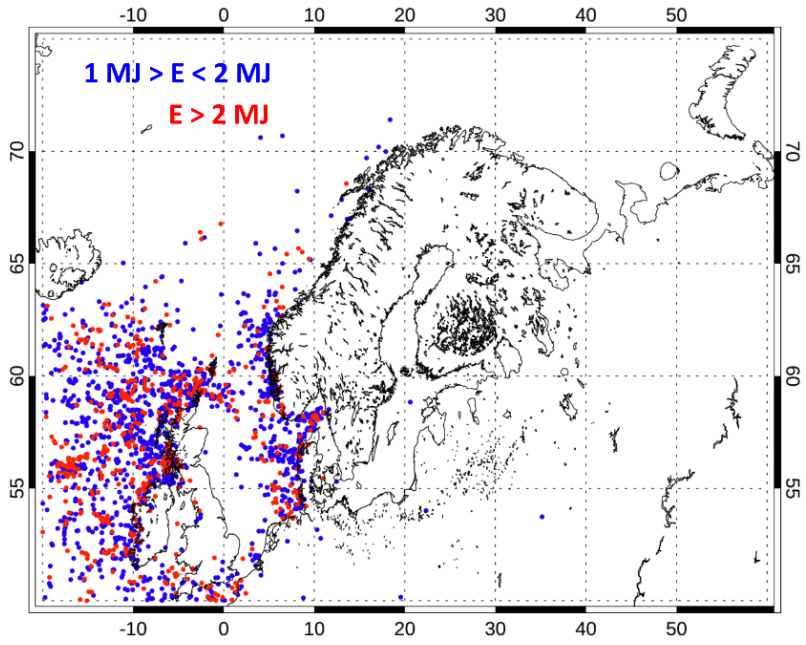

Spatial distribution of superbolts (strokes with energies of 1–2 MJ and above 2 MJ are represented by the blue and red points, respectively).

Reference:

Kolmašová, I., **Santolík, O.**, and **Rosická, K.** (2022), Lightning activity in northern Europe during a stormy winter: disruptions of weather patterns originating in global climate phenomena, *Atmos. Chem. Phys.*, 22, 3379-3389. doi:10.5194/acp-22-3379-2022.

Related reference:

Peterson, M. J., Lang, T. J., Logan, T., Wee Kiong, C., Gijben, M., Holle, R., **Kolmašová, I.**, Marisaldi, M., Montanya, J., Pawar, S. D., Zhang, D., Brunet, M. and Cerveny, R. S. (2022), New WMO Certified Megaflash Lightning Extremes for Flash Distance (768 km) and Duration (17.01 seconds) Recorded from Space, *Bulletin of the American Meteorological Society*. doi:10.1175/BAMS-D-21-0254.1.

4. A frontal thunderstorm with several multi-cell lines found to produce energetic preliminary breakdown

We combine electromagnetic measurements with meteorological and lightning detection data to explain an observation of unusually strong preliminary breakdown (PB) produced by a thunderstorm system that developed along the Mediterranean Coast of Southern France in the early hours of 19 June 2013. This multi-cellular storm was composed of several parallel convective lines in the NW-SE direction. Our analysis focuses on ten sequences of energetic electromagnetic PB pulses recorded by two receivers located at different distances from this thunderstorm. The peak currents, which generated these strong PB pulses, reached -36 kA. The initial polarity of all observed energetic PB pulses confirmed the movement of the negative charge downward, as in case of PB pulses preceding negative cloud-to-ground discharges. The locations of PB pulses appeared in areas with none or very

weak lightning activity. Most PB pulses were initiated in small, short-living, rapidly moving convective storm cells characterized by low reflectivity values (generally < 40 dBZ), weak vertical development, and low flash density. Our findings indicate that the observed thunderstorm might posses temporary strong negatively charged pockets located above a strong positive charge region at low-level. Such charge arrangement, likely explains our observation of unusually strong PB pulses and the absence of RS pulses in electromagnetic recordings.

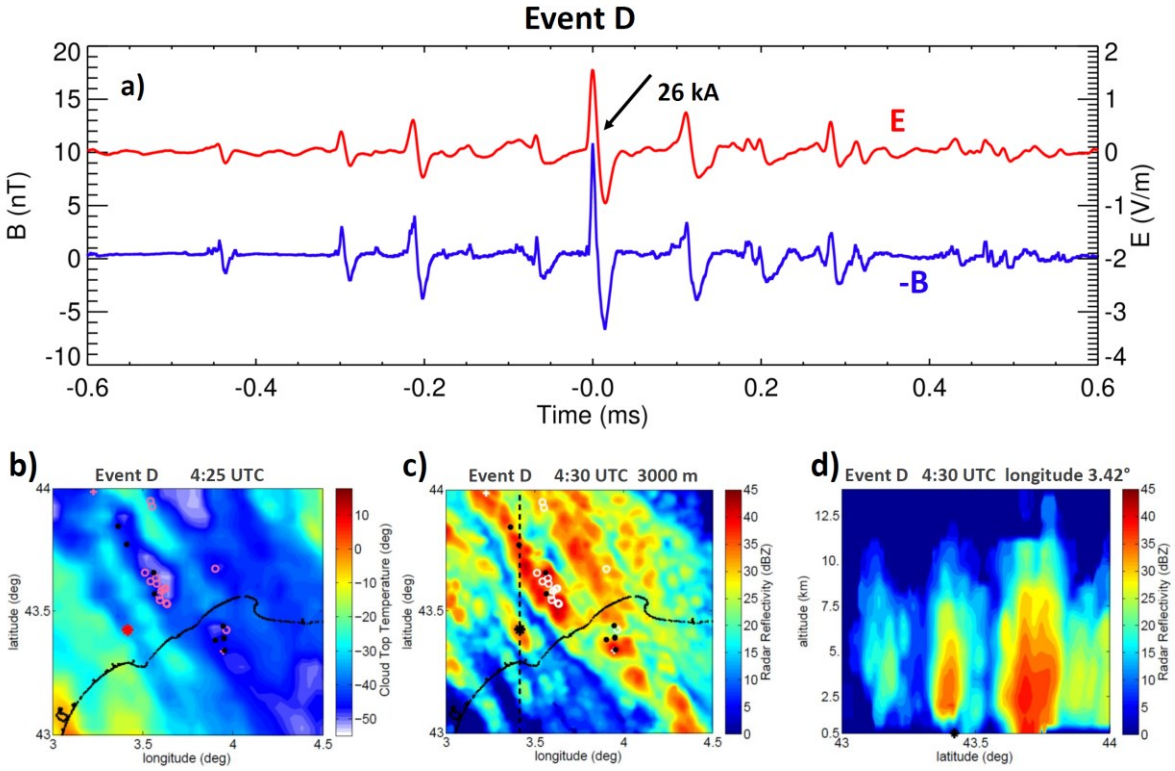

a) An example of magnetic-field (blue line) and electric-field waveforms (red line) of a train of PB pulses (event D) shifted in time to have the strongest PB pulse at t=0. The PB pulse reported by EUCLID is indicated by black arrows together with its peak current estimate; b) CTT in Celsius at the time indicated; c) horizontal cross section of radar reflectivity in dBZ at 3000 m of altitude; d) vertical cross section of radar reflectivity along the black dashed line in c).

Reference:

Kolmašová, I., Soula, S., **Santolík, O.**, Farges, T., Bousquet, O., Diendorfer, G., et al. (2022). A frontal thunderstorm with several multi-cell lines found to produce energetic preliminary breakdown. *Journal of Geophysical Research: Atmospheres*, 127. doi:10.1029/2021JD035780.

Related references:

Scholten, O., Hare, B. M., Dwyer, J., Liu, N., Sterpka, C., **Kolmašová, I.**, **Santolík**, **O., Lán**, **R., Uhlíř**, **L.**, S. Buitink, T. Huege, A. Nelles, and S. ter Veen (2022). Interferometric imaging of intensely radiating negative leaders. *Phys. Rev. D* 105, 062007. doi:10.1103/PhysRevD.105.062007.

Liu, N. Y., Scholten, O., Hare, B. M., Dwyer, J. R., Sterpka, C. F., **Kolmašová, I**., & **Santolík, O.** (2022). LOFAR observations of lightning Initial breakdown pulses. *Geophysical Research Letters*, 49. doi:10.1029/2022GL098073.

5. Continental thunderstorm ground enhancement observed at an exceptionally low altitude

Two long-lasting Thunderstorm Ground Enhancement (TGE) events were registered at the Milešovka meteorological observatory in Czechia (50.55N, 13.93E, altitude 837 m) on 23 April 2018, during linearly organized thunderstorms. Two intervals of increased gamma ray photon counts were detected by a plastic scintillator, respectively lasting 70 and 25 minutes, and reaching 31% and 48% above the background radiation levels. Using numerical simulations, we verified that the observed increases of count rates are consistent with the energy spectrum of previously observed TGEs. We investigated the relevant data from a suite of meteorological instruments, a Ka-band cloud radar, an electric field mill, and a broadband electromagnetic receiver, all placed at the Milešovka observatory, in order to analyze the context in which these unique continental TGEs occurred at an exceptionally low altitude. The onset of the TGEs preceded the onset of precipitation by 10 and 3 minutes, respectively, for the two events. Both this delayed rain arrival and a lower energy threshold of 6.5 MeV for registered particles clearly exclude the detection the decay products of the radon progeny washout during the TGE intervals. At the same time, the European lightning detection network EUCLID detected numerous predominantly negative intracloud lightning discharges at distances closer than 5 km from the particle detector, while the occurrence of cloud-to-ground discharges was suppressed. The cloud radar recorded presence of graupel below the melting level and the composition of hydrometeors suggested good conditions for cloud electrification. The observed variations of the near surface electric field were unusual, with very brief negative electric field excursions reaching -20 kV in a quick succession. At the same time, sub-microsecond unipolar pulses emitted by close corona discharges saturated the broadband magnetic loop antenna. All these measurements indicate that a strong lower positive charge region was present inside the thundercloud. The lower thundercloud dipole was probably responsible for acceleration of the seed electrons in the air. These seed electrons might originate not only in the secondary cosmic ray particles but could also come from a high concentration of radon in the air collected during the propagation of the convective system above the uranium-rich soils before the thunderstorms overpassed the Milešovka observatory.

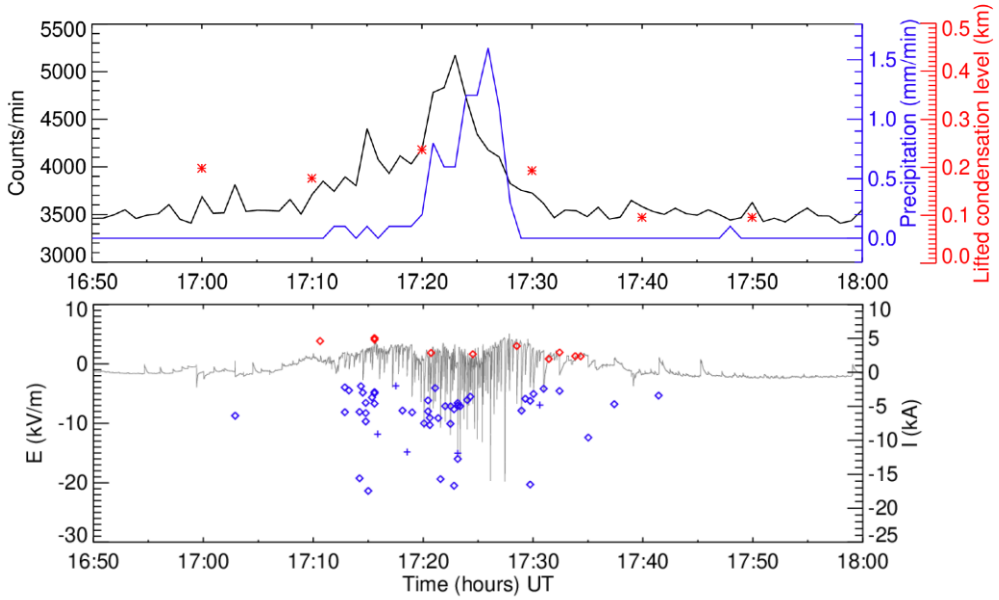

a) Particle counts per minute (black line), precipitation totals in mm/min (blue line), the altitudes of the lifted condensation level in km above Milešovka observatory (red stars); b) fluctuations of the

vertical electric field measured by electric field mill (grey line), EUCLID detections: red and blue color for positive and negative discharges, diamonds for IC discharges and crosses for CG discharges.

Reference:

Kolmašová, I., **Santolík, O.**, Šlegl, J., Popová, J., Sokol, Z., Zacharov, P., Ploc, O., Diendorfer, G., Langer, R., **Lán, R.**, and Strhárský, I. (2022), Continental thunderstorm ground enhancement observed at an exceptionally low altitude, *Atmos. Chem. Phys.*, 22, 7959-7973. doi:10.5194/acp-22-7959-2022.

6. Model of the First Lightning Return Stroke Using Bidirectional Leader Concept

We have developed a new lightning return stroke model which takes into account a realistic charge distribution to compute the ambient electric potential. It contains a nonlinear resistance model for the development of the finite conductivity of the lightning channel. It also describes a redistribution of charges after the bottom end of the channel is attached to the potential of the ground. The model is based on solving Maxwell's equations linked to Poisson's equation, and coupled with Ohm's law. The waveshape of the current at the channel base is obtained from the model. The simulated current decreases and its rise time increases with height, which is in accordance with the luminosity observations. The electric and magnetic field waveforms modeled for different distances from the lightning flash show that most of the waveform features typically observed at these distances are well reproduced. We also successfully compare modeled magnetic field waveforms with measurements at the distances larger than 30 km**.**

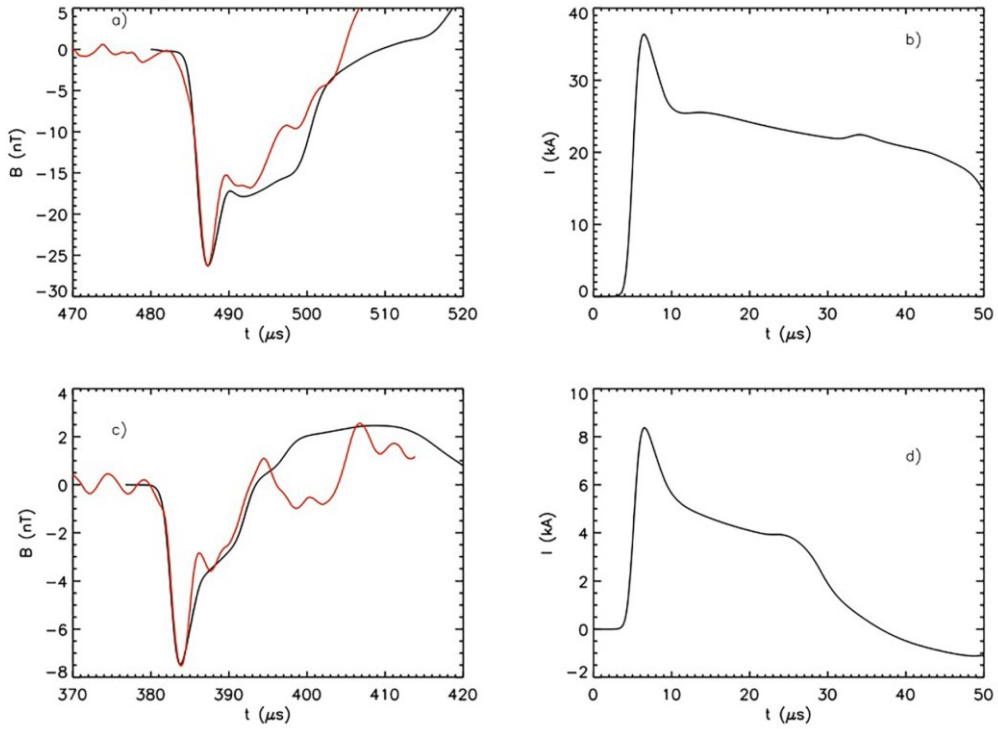

Modeled RS waveforms (black lines) compared with measurements (red lines) together with derived channel-base currents. The measured distances from the RS channel are: (a) 144 km, (c) 113 km. The peak currents estimated by the lightning location network Météorage were 59 and 12 kA.

Reference:

Kašpar, P., Kolmašová, I., & Santolík, O. (2022). Model of the first lightning return stroke using bidirectional leader concept. Journal of Geophysical Research: Atmospheres, 127, e2022JD037459. https://doi.org/10.1029/2022JD037459

7. Classification of spectral fine structures of Saturn kilometric radiation

The spectral fine structures of Saturn kilometric radiation (SKR) are best investigated with the wideband receiver (WBR) of Cassini's Radio and Plasma Wave Science (RPWS) instrument, with which measured radio fluxes can be displayed in time–frequency spectra with resolutions of 125 ms and ~ 0.1 kHz. We introduce seven different classes of SKR fine structures ranging from dots (one class for 0-dimensional objects) over lines (four classes of 1-dimensional objects being horizontal, vertical, or with negative or positive slope) to areal features (one class for 2-dimensional objects). Additionally, we define a seventh class containing special structures named according to their appearance in time–frequency spectra. These special features are named rain, striations, worms, and caterpillar and the latter two have never been described in the literature so far. Using this newly defined classification scheme, we classify features in spectra at low frequencies in the baseband of the 80 kHz WBR and at medium frequencies around 325 kHz. A statistic of the occurrence of various classes and sub-classes shows some notable characteristics: lines with a positive slope are much more common at medium frequencies than at low frequencies and vertical lines are almost absent at low frequencies. The particular fine structure of striations (group of narrowbanded lines with predominantly negative slopes) is quite common below 80 kHz but less common near 325 kHz. At these medium frequencies, the lines rather look like interrupted striations which we term with the name "rain". We also find rare instances of striations with a positive slope and rare instances of absorption signatures within areal features. The newly introduced sub-classes of worms (lines oscillating in frequency) and caterpillars occur almost exclusively below 80 kHz. Caterpillars have a typical bandwidth of 10 kHz, a constant frequency below ~ 40 kHz for several hours and they are mostly observed beyond distances of 10 Saturn radii. We discuss the implications of our findings in view of the many theories about spectral fine structures of auroral radio emissions.

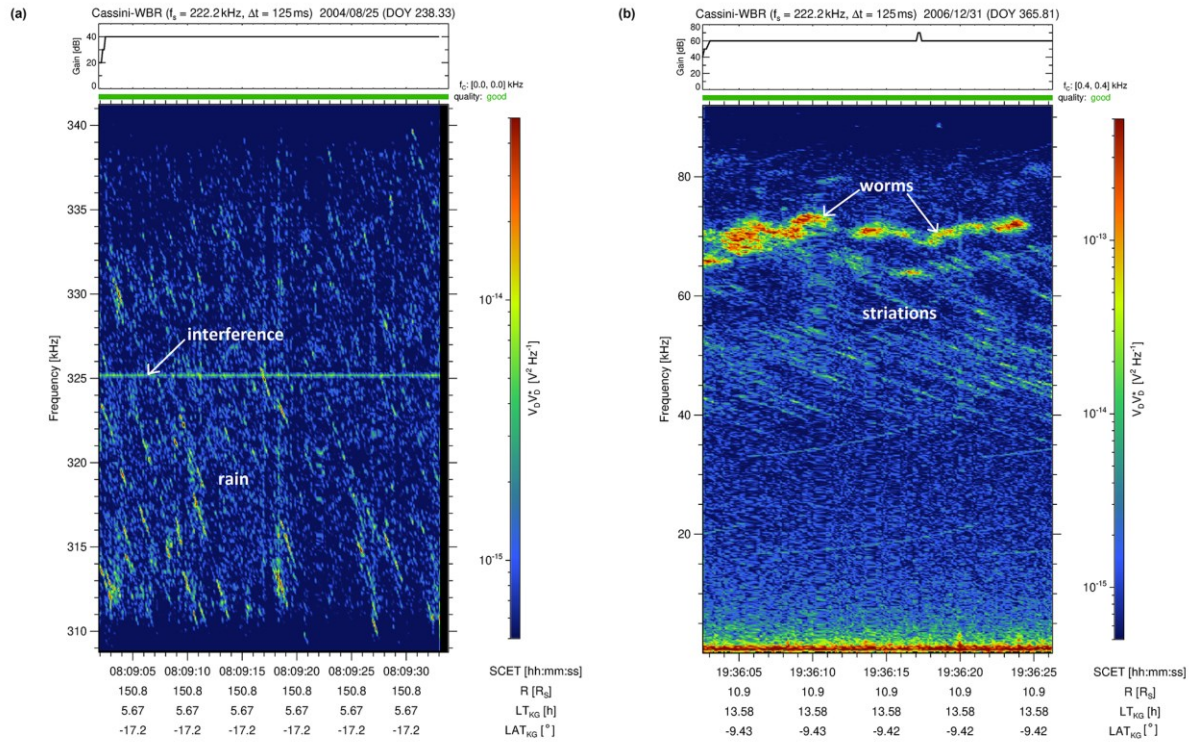

SKR fine structures called "rain" at 325 kHz in comparison to "striations" at 80 kHz measured by the Cassini WBR. Above 60 kHz, the newly defined features called worms can be seen.

Reference:

Fischer, G., **U. Taubenschuss**, and **D. Píša**, Classification of spectral fine structures of Saturn kilometric radiation (2022), *Ann. Geophys.*, 40, 485-501. doi:10.5194/angeo-40-485-2022.

Related references:

Parrot, M., Němec, F., & **Santolík, O.** (2022). Properties of AKR-like emissions recorded by the low altitude satellite DEMETER during 6.5 years. *Journal of Geophysical Research: Space Physics*, 127. doi:10.1029/2022JA030495.

Wu, S., Zarka, P., Lamy, L., **Taubenschuss, U.**, Cecconi, B., Ye S. Y., Fischer, G., Kurth, W. S., and Francez, T. (2022), Observations of the first harmonic of Saturn Kilometric Radiation during Cassini's Grand Finale, *Journal of Geophysical Research: Space Physics*, 127. doi:10.1029/2022JA030776.

Wu, S., Ye, S. Y., Fischer, G., **Taubenschuss, U.**, Jackman, C. M., O'Dwyer, E., Kurth, W. S., Yao, S., Yao, Z. H., Menietti, J. D., Xu, Y., Long, M. Y., and Cecconi, B. (2022), Saturn Anomalous Myriametric Radiation, a new type of Saturn radio emission revealed by Cassini, *Geophys. Res. Lett*., 49, 16. doi:10.1029/2022GL099237.

Sulaiman, A. H., Mauk, B. H., Szalay, J. R., Allegrini, F., Clark, G., Gladstone, G. R., Kotsiaros, S., Kurth, W. S., Bagenal, F., Bonfond, B., Connerney, J. E. P., Ebert, R. W., Elliott, S. S., Gershman, D. J., Hospodarsky, G. B., Hue, V., Lysak, R. L., Masters, A., **Santolík**, **O.,** Saur, J, and Bolton, S. J. (2022). Jupiter's low-altitude auroral zones: Fields, particles, plasma waves, and density depletions. *Journal of Geophysical Research: Space Physics*, 127. doi:10.1029/2022JA030334.

Kurth, W. S., Sulaiman, A. H., Hospodarsky, G. B., Menietti, J. D., Mauk, B. H., Clark, G., F. Allegrini, P. Valek , J. E. P. Connerney, J. H. Waite , S. J. Bolton, M. Imai, **O. Santolik,** W. Li, S. Duling, J. Saur, and C. Lou (2022). Juno plasma wave observations at Ganymede. Geophysical Research Letters, 49, e2022GL098591. https://doi.org/10.1029/2022GL098591

8. Alpha transmitter signals observed by the Van Allen Probes: Ducted versus nonducted propagation

The interaction of very low frequency transmitter signals with radiation belt electrons depends ultimately on their wave normal angles. In the equatorial interaction region, these can be either low (ducted propagation) or comparatively large (nonducted propagation). Experimentally distinguishing the two modes is complicated, as multicomponent spacecraft data typically do not extend to high enough frequencies with a sufficient frequency resolution. One exception that we exploit are 11.9 kHz signals from Alpha transmitters detectable by the Van Allen Probes spacecraft. We use multicomponent burst mode measurements to distinguish between the ducted and nonducted modes of propagation and to evaluate their relative importance. While the ducted waves are detected less often, they tend to have larger Poynting fluxes. The total power propagating in the two modes is thus comparable. Magnetic local time and in-situ density fluctuations are main parameters controlling the relative fraction of ducted waves.

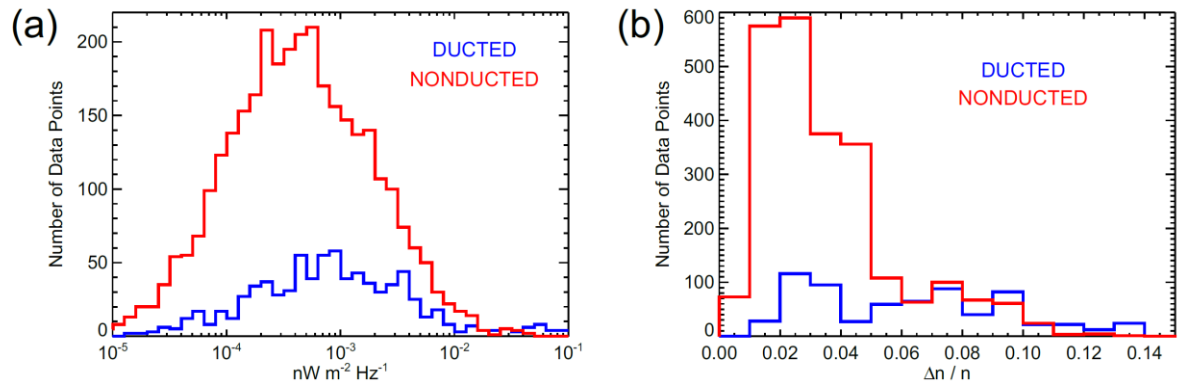

(a) Histograms of Poynting fluxes during the time intervals when the signal propagation is classified as ducted/non-ducted are shown by the blue/red lines, respectively. (b) The same as (a), but for histograms of plasma number density fluctuations.

Reference:

Němec, F., **Santolík, O.**, Hospodarsky, G. B., & Kurth, W. S. (2022). Alpha transmitter signals observed by the Van Allen Probes: Ducted versus nonducted propagation. *Geophysical Research Letters*. 49. doi:10.1029/2022GL098328.

Related reference:

Němec, F., **Santolík, O.**, Hospodarsky, G. B., Kurth, W. S., & Kletzing, C. A. (2022). Power Line Harmonic Radiation observed by the Van Allen Probes spacecraft. *Journal of Geophysical Research: Space Physics*, 127. doi:10.1029/2022JA030320.

9. Over-expansion of coronal mass ejections modelled using 3D MHD EUHFORIA simulations

Coronal mass ejections (CMEs) are large-scale eruptions observed close to the Sun. They travel through the heliosphere and possibly interact with the Earth environment, creating interruptions or even damaging new-technology instruments. Most of the time their physical conditions (velocity, density and pressure) are measured in situ at only one point in space, with no possibility of having information on the variation of these parameters during their journey from the Sun to Earth. Aim: Our aim is to understand the evolution of the internal physical parameters of a set of three particular fast halo CMEs. These CMEs were launched between 15 and 18 July 2002. Surprisingly, the related interplanetary CMEs (ICMEs), observed near Earth, have a low, and in one case a very low, plasma density. Method: We use the EUropean Heliospheric FORecasting Information Asset (EUHFORIA) model to simulate the propagation of the CMEs in the background solar wind by placing virtual spacecraft along the Sun–Earth line. We set up the initial conditions at 0.1 au, first with a cone model and then with a linear force-free spheromak model. Results: Relatively good agreement between the simulation results and observations concerning the speed, density and arrival times of the ICMEs is obtained by adjustment of the initial CME parameters. In particular, this is achieved by increasing the initial magnetic pressure so that a fast expansion is induced in the inner heliosphere. This resulted in the development of fast expansion for two of the three ICMEs. In contrast, the intermediate ICME is strongly overtaken by the last ICME, so its expansion is strongly limited.

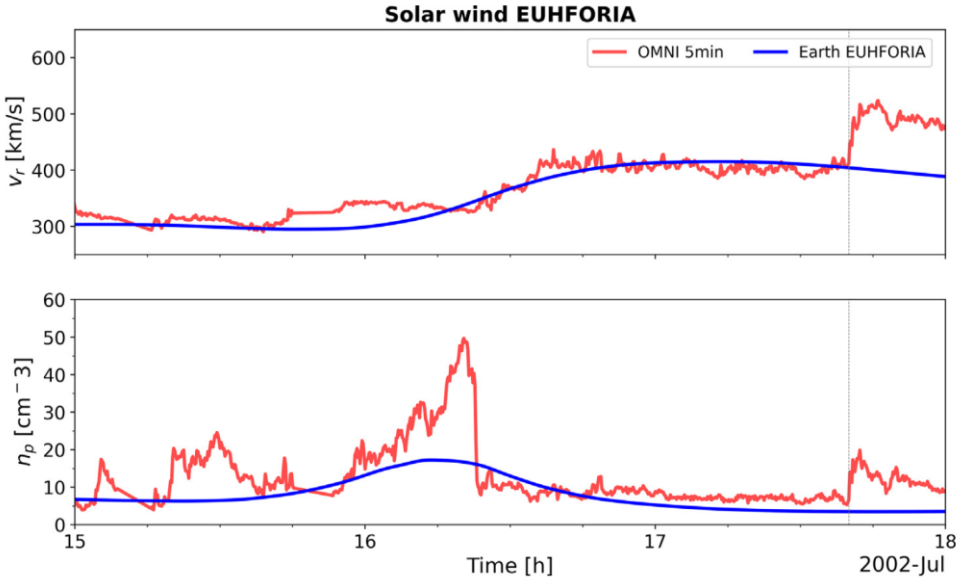

EUHFORIA best results for the solar wind computed at L1 (blue curves) between 15 and 18 July 2002 compared with in situ measurements at L1 (red curves).

Reference:

Verbeke, C., Schmieder, B, Démoulin, P., Dasso, S., **Grison, B.**, Samara, E., Scolini, C., and Poedts, S. (2020), Over-expansion of coronal mass ejections modelled using 3D MHD EUHFORIA simulations, *Advances in Space Research*, Vol. 70, Issue 6, 1663-1683. doi:10.1016/j.asr.2022.06.013.

Related reference:

Dimmock, A. P., Khotyaintsev, Yu. V., Lalti, A., Yordanova, E., Edberg, N. J. T., Steinvall, K., , D. B., Graham , Hadid, L. Z., Allen, R. C. Vaivads, A., Maksimovic, M. Bale, S. D., Chust, T., **Souček, J.** et al. (2022), Analysis of multiscale structures at the quasi-perpendicular Venus bow shock, *A&A* 660, A64. doi: 10.1051/0004-6361/202140954.

O. Mousis, O., Bouquet, A., Langevin, Y., André, N., Boithias, H., Durry, G., Faye, F., Hartogh, P., Helbert, J., Iess, L , Kempf, J., Masters, A., Postberg, F., Renard, J.-B., Vernazza, P., Vorburger, A., Wurz, P., Atkinson, D. H., Barabash, S., **Kolmašová, I.** et al. (2022), Moonraker: Enceladus Multiple Flyby Mission, *The Planetary Science Journal*, 3:268. doi.org/10.3847/PSJ/ac9c03.

10. Transmission of foreshock waves through Earth's bow shock

The Earth's magnetosphere and its bow shock, which is formed by the interaction of the supersonic solar wind with the terrestrial magnetic field, constitute a rich natural laboratory enabling in situ investigations of universal plasma processes. Under suitable interplanetary magnetic field conditions, a foreshock with intense wave activity forms upstream of the bow shock. So-called 30 s waves, named after their typical period at Earth, are the dominant wave mode in the foreshock and play an important role in modulating the shape of the shock front and affect particle reflection at the shock. These waves are also observed inside the magnetosphere and down to the Earth's surface, but how they are transmitted through the bow shock remains unknown. By combining state-of-the-art global numerical simulations and spacecraft observations, we demonstrate that the interaction of foreshock waves with the shock generates earthward-propagating, fast-mode waves, which reach the magnetosphere. These findings give crucial insight into the interaction of waves with collisionless shocks in general and their impact on the downstream medium.

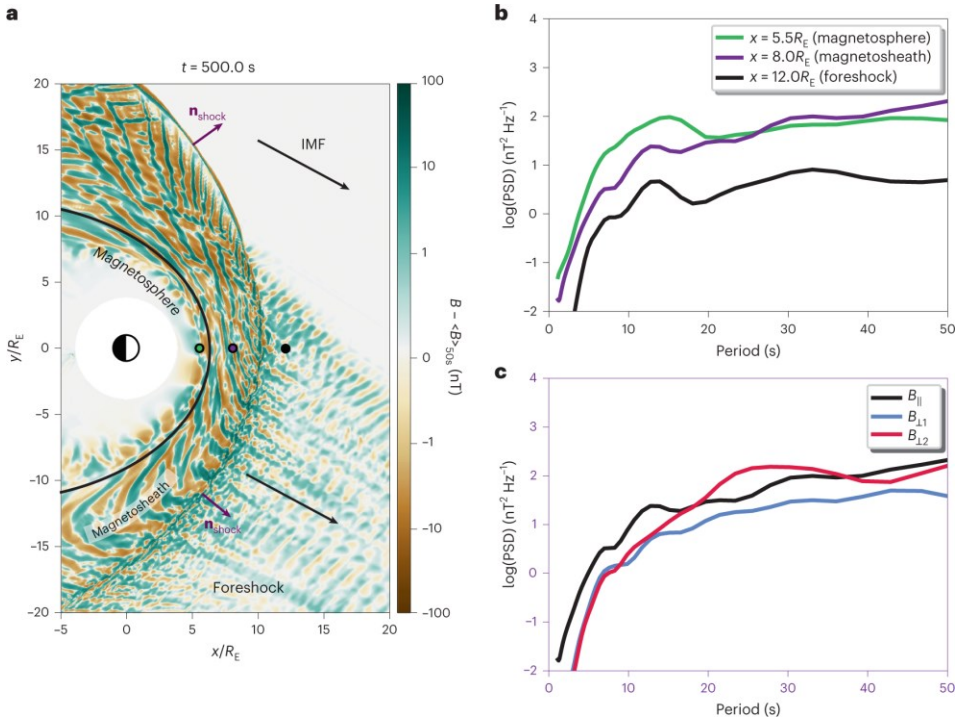

Overview of the simulation and wave activity in the foreshock and magnetosheath. (a) Color map of the magnetic field strength fluctuations in the simulation plane at time t = 500 s from the beginning of the simulation. We subtract <B>50s, which is a 50 s average of the field magnitude, from B to reveal the fluctuations of the magnetic field magnitude. The black curve shows the approximate magnetopause location. The black arrows show the IMF direction, and the purple arrows depict the shock normal direction n_{shock} at two positions along the bow shock. (b) PSD of the total magnetic field fluctuations at the three locations marked by colored circles in a. (c) PSD of the magnetic field fluctuations parallel and perpendicular to the mean magnetic field at the virtual spacecraft location

in the magnetosheath. The perpendicular directions are defined such that B⊥1 lies in the simulation (x–y) plane while B⊥2 completes the right-handed set.

Reference: Turc, L., O. W. Roberts, D. Verscharen, A. P. Dimmock, P. Kajdič, M. Palmroth, Y. Pfau-Kempf1, A. Johlander, M. Dubart, E. K. J. Kilpua, **J. Souček**, K. Takahashi, N. Takahashi, M. Battarbee, and U. Ganse (2022), Transmission of foreshock waves through Earth's bow shock, *Nature Physics*, 1745-2481, doi:10.1038/s41567-022-01837-z.

Department of Space Physics, Institute of Atmospheric Physics of the Czech Academy of Sciences in 2022

1. Samuel Amrich, student, 20% FTE
2. Radka Balková, secretary, 50% FTE
3. Sampath Bandara, postdoctoral associate, till 28 February 2022
4. Benjamin Grison, research scientist
5. Michajlo Hajoš, research scientist
6. Miroslav Hanzelka, PhD student, 70% FTE, since 6 June postdoc., since 1 August on leave
7. Jiří Jánský, research engineer
8. Petr Kašpar, research scientist
9. Ivana Kolmašová, senior research scientist
10. Andrea Kolínská, PhD student, 70% FTE
11. *Vratislav Krupař, research scientist, on leave*
12. *Oksana Krupařová, research scientist, on leave*
13. Radek Lán, research engineer
14. Ján Mičko, PhD student, 70% FTE, since 1 October
15. David Píša, research scientist
16. Martin Popek, TLE observer, 25% FTE
17. Kateřina Rosická, student, 20% FTE
18. Ondřej Santolík, senior research scientist, head of the department
19. Jan Snížek, research engineer, 50% FTE
20. Jan Souček, senior research scientist, deputy head of the department
21. *Hana Špačková, on leave*
22. Ulrich Taubenschuss, research scientist
23. *Alexander Tomori, PhD student, on leave*
24. Marie Turčičová, postdoctoral associate, 80% FTE
25. Luděk Uhlíř, research engineer